(Received 3 December 2024, Accepted 19 December 2024, Scheduled 20 December 2024)

Reflectionless Refraction via One-Dimensional Ghost Polaritons in Planar Junctions of Hyperbolic Metasurfaces

Zhiwei He[1,2,3], Huaping Wang[1,2,3,*], Zhenyang Cui[1,2,3], Sihao Xia[1,2,3], Xingyu Tang[1,2,3], Bin Zheng[1,2,3], Xiao Lin[1,2,3], Lian Shen[1,2,3], Hongsheng Chen[1,2,3], and Yingjie Wu[1,2,3,*]

[1]*ZJU-Hangzhou Global Science and Technology Innovation Center*
Key Laboratory of Ocean Observation-Imaging Testbed of Zhejiang Province
Ocean College, Zhejiang University, Hangzhou 310058, China
[2]*Interdisciplinary Center for Quantum Information, State Key Laboratory of Extreme Photonics and Instrumentation*
College of Information Science and Electronic Engineering, Zhejiang University, Hangzhou 310027, China
[3]*Key Laboratory of Advanced Micro/Nano Electronic Devices & Smart Systems of Zhejiang*
Jinhua Institute of Zhejiang University, Zhejiang University, Jinhua 321099, China

ABSTRACT: Polaritons, part-light-part-matter waves, enable the control of light at the subwavelength scale. Interfacial behaviors play a critical role in polariton manipulation, with negative refraction showing promise for high-resolution focusing. However, reflections pose a substantial challenge, especially in applications where backscattering is unwanted. To address this issue, we propose a structure composed of planar junctions of metasurfaces, each supporting in-plane hyperbolic polaritons with misaligned optical axes. We demonstrate that when the asymptote of the incident hyperbolic isofrequency contours (IFCs) aligns with the interface normal, the reflected waves transform into highly lossy one-dimensional ghost polaritons (HL-1DGPs), channeling energy near the interface. The refracted waves also convert into HL-1DGPs when the outgoing IFC asymptote aligns with the interface normal. Leveraging these phenomena, we design polaritonic lenses and absorbers with greatly reduced reflection. These insights into the interfacial behaviors of hyperbolic polaritons under symmetry breaking have implications for creating polaritonic elements beyond the diffraction limit.

1. INTRODUCTION

Polaritons represent a unique class of interface waves originating from light-matter interactions [1–4]. Owing to their strong field localization capabilities, polaritons provide an optimal platform for controlling electromagnetic fields at the extreme scale [5, 6], enabling the development of waveguides [7–11], prisms [12–14], lenses [15–22], and other polaritonic elements with resolutions far beyond the diffraction limit [23]. Refraction in polaritonic systems occurs as polaritons cross interfaces between two media with distinct effective indices. Particularly, negative refraction can enhance focusing resolution by directing refracted energy flux on the same side of the interface normal as the incident polaritons [24]. Negative refraction of polaritons has been demonstrated in both theoretical [25–33] and experimental studies [34–37]; however, it often coincides with undesired reflections, which pose a challenge for applications relying on refraction-based polaritonic elements. Mitigating these reflections is therefore highly desirable but remains challenging.

In light of momentum conservation along the interface, an open isofrequency contour (IFC), also known as equifrequency contour, is crucial for achieving reflectionless refraction. This concept has been validated in photonic Weyl systems featuring surface arc states [38, 39]. In such systems, electromagnetic waves with hyperbolic IFCs could eliminate reflection during refraction under appropriate conditions [40]. While similar mechanisms have been explored in the microwave range [41, 42], their application to polaritonic systems has received limited attention. Given that polaritons as evanescent waves require additional considerations in the out-of-plane direction when their IFCs are calculated [43], which complicates the rigorous analysis of their behavior at interfaces.

Here, we theoretically investigate the interfacial behavior of hyperbolic polaritons with slanted optical axes, with special emphasis on cases where hyperbolic IFC asymptotes align with the interface normal. We find that when the incident or outgoing IFCs are rotated by a specific angle, the reflected and refracted polaritons transform into highly lossy one-dimensional ghost polaritons (HL-1DGPs), channeling their energy near the interface. This insight could inform the design of reflection-resistant polaritonic lenses and absorbers, providing new directions for the subwavelength light control in planar polaritonic devices.

2. RESULTS

We first consider the refraction and reflection behaviors of polaritons, which can be understood geometrically via IFCs. These contours represent the projection of wavevectors (**k**) at a given frequency (ω) and are schematically illustrated in Fig. 1. Here, we take in-plane hyperbolic polaritons with positive dispersion as the incidence ($\frac{d\omega}{dk_1} > 0$). Solid blue curves in

* Corresponding authors: Huaping Wang (hpwang@zju.edu.cn); Yingjie Wu (yingjie.wu@zju.edu.cn).

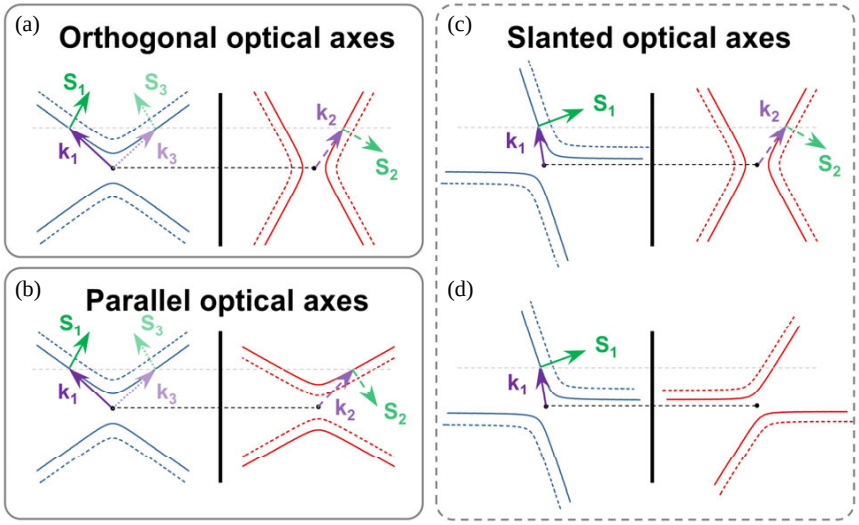

FIGURE 1. IFC analysis of the interfacial behaviors of polaritons. (a) Negative refraction between hyperbolic polaritons with orthogonal optical axes, where both dispersions are positive, $\frac{d\omega_1}{dk_1} \cdot \frac{d\omega_2}{dk_2} > 0$, but the slopes are opposite, $\frac{dk_{y1}}{dk_{x1}} \cdot \frac{dk_{y2}}{dk_{x2}} < 0$. (b) Negative refraction between hyperbolic polaritons with parallel optical axes, where $\frac{d\omega_1}{dk_1} \cdot \frac{d\omega_2}{dk_2} < 0$ and $\frac{dk_{y1}}{dk_{x1}} \cdot \frac{dk_{y2}}{dk_{x2}} < 0$. (c), (d) IFC analysis of interfaces between hyperbolic polaritons with slanted optical axes. Reflection is expected to be forbidden when the asymptote of the incident IFC aligns with the interface normal (c). When the asymptotes of both the incident and outgoing IFCs align with the interface normal (d), both reflection and refraction appear to be prevented, which is physically implausible. Black solid lines represent interfaces. Solid, dashed, and dotted purple (green) arrows denote the incident, refracted, and reflected wavevectors (Poynting vectors), respectively.

Fig. 1(a) depict the corresponding IFC, while dashed curves indicate the IFC at a slightly higher frequency. For anisotropic polaritons, the directions of **k** and Poynting vectors (**S**) are usually non-collinear, meaning that they do not align, except when k_x or k_y equals zero. For high-k approximations, **S** is normal to IFCs, and it points to the negative y direction when the slope of the incident IFC is positive, $\frac{dk_y}{dk_x} > 0$, and vice versa.

Upon encountering an interface (black line in Fig. 1), causality dictates that refracted power flows outward, while reflected power flows back toward the source [44]. Using IFCs, we can derive refraction and reflection behaviors geometrically based on interface wavevector conservation, as shown in Fig. 1. The direction of the refracted Poynting vector ($\mathbf{S}_2$) is determined by the slope of the IFC in the outgoing medium ($\frac{dk_{2y}}{dk_{2x}}$), following a similar mechanism to $\mathbf{S}_1$ in the incident medium. Comparing the directions of $\mathbf{S}_1$ and $\mathbf{S}_2$, it might be safe to conclude that at a y-oriented interface, positive refraction occurs when $\frac{dk_{1y}}{dk_{1x}} \cdot \frac{dk_{2y}}{dk_{2x}} > 0$, while negative refraction takes place when $\frac{dk_{1y}}{dk_{1x}} \cdot \frac{dk_{2y}}{dk_{2x}} < 0$. This principle applies to both positive and negative dispersion polaritons and holds for both open and closed IFCs. In previous works, however, negative dispersion ($\frac{d\omega}{dk} < 0$), also referred to as negative group velocity, was often required for negative refraction due to similar incident and outgoing IFC topologies (Fig. 1(b)) [27, 30, 45, 46]. However, this constraint can be relaxed when IFCs undergo topological transitions [28, 31–36].

The reflected wavevectors ($\mathbf{k}_3$) and Poynting vectors ($\mathbf{S}_3$) can be similarly derived. In the cases shown in Figs. 1(a), (b), negative refractions are accompanied by reflections because there are always intersections between the interface normals and IFCs, indicating a real solution for $\mathbf{k}_3$. However, due to the open nature of the incident hyperbolic IFCs, it seems that if the interface normal is in line with the asymptotes of hyperbolas (Fig. 1(c)), no intersection occurs, suggesting that reflection should be forbidden. Consequently, if one of the asymptotes of the outgoing hyperbolas is also parallel to the interface normal, both refraction and reflection seem impossible (Fig. 1(d)). However, this deduction violates energy conservation, indicating that the above interfacial matching condition cannot be established solely based on current IFC analysis. Previous studies have suggested that reflected flow along the interface could be a potential solution [31, 47], but a rigorous analysis has been lacking, which is the focus of this work.

We attribute the above paradox to the formation of recently proposed one-dimensional ghost polaritons (1DGPs), with their energy dissipating along a direction close to the interface. To verify this hypothesis, we consider a realistic structure composed of laterally arranged hBN ribbon arrays. It has been proposed and demonstrated that such metasurfaces can introduce symmetry breaking in isotropic systems, leading to in-plane hyperbolic polaritons [48–50]. The left and right metasurfaces of the y-oriented interface are designed to support in-plane hyperbolic polaritons with different orientations. The geometric parameters are detailed in the caption of Fig. 2(a). Compared to natural materials that support in-plane hyperbolic polaritons, this structure provides new tuning knobs for polaritons, i.e., geometric parameters, and avoids potential gaps or steps between the two metasurfaces and could be fabricated within a monolithic hBN slab using lithography followed by an etching process [49, 50].

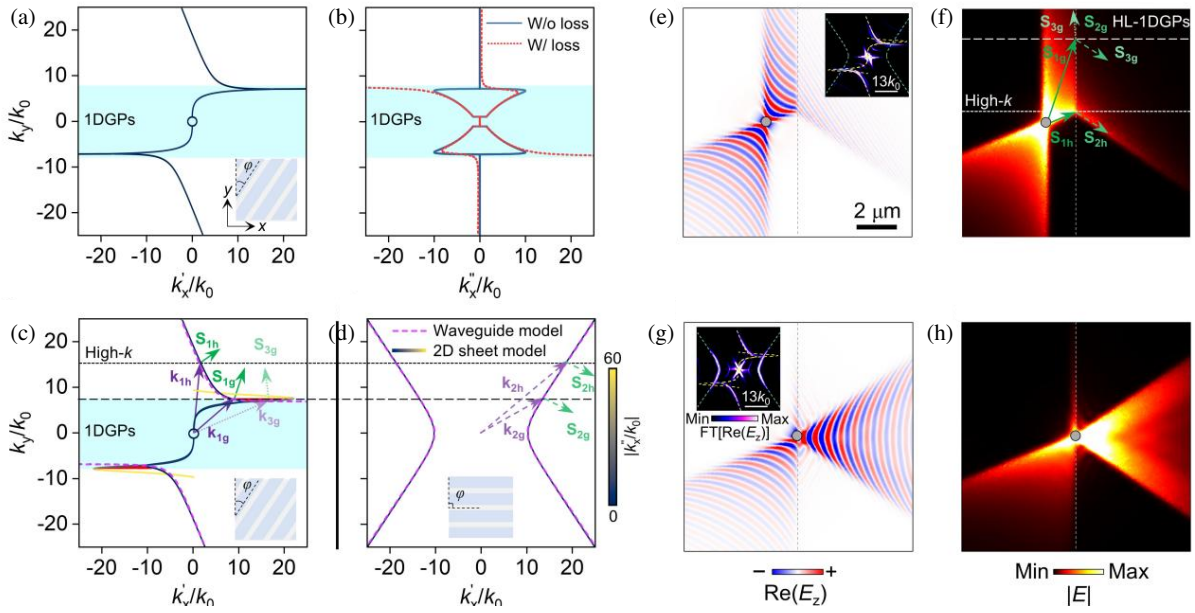

FIGURE 2. IFC analysis based on HL-1DGPs. (a) Real part of the IFCs calculated by modelling the slanted hBN metasurfaces as a 2D conductive sheet, with the cyan area representing the 1DGP region. Inset shows a schematic (top view) of the slanted hBN metasurfaces, with the thickness (d), width (w), gap (g), and period (p) of 20, 60, 40, and 100 nm, respectively. The oblique angle (φ) is 34°. The imaginary part of the wavevectors $\left(\left|k_x''/k_0\right|\right)$ is color-coded. The central circle corresponds to the IFC of free-space light with the wavevector of k_0. (b) Corresponding imaginary IFCs. (c) Real IFC for the same structure as in (a), but including the intrinsic material loss, showing two HL-1DGP subregions (red areas) within the 1DGP region. (d) Calculated IFC with its transverse axis parallel to the y axis, i.e., $\varphi = 90°$. Two models are used for the analytical calculation: a 2D conductive sheet (blue-yellow curves) and a three-layer waveguide (pink curves). IFC analyses based on the matching condition are conducted at high-k region (black dotted line) and HL-1DGP region (black dashed line). (e) Simulated electric field distribution, represented by Re(E_z). A z-polarized dipole (gray dot) is placed 1.5 μm to the left of the interface (gray line). Inset shows the Fourier transform (FT) spectrum, quantitatively matching the calculated incident (yellow) and outgoing (green) IFCs. (f) Corresponding simulation result for the magnitude of the electric field. (g), (h) Same as (e), (f) except that the point dipole is placed at the interface.

We first investigate the scenario depicted in Fig. 1(c), where one of the asymptotes of the incident IFC is parallel to the x axis. To quantitatively calculate IFCs, we model hBN metasurfaces as two-dimensional (2D) conductive sheets with surface conductivity tensor $\overline{\overline{\sigma}} = -id\varepsilon_0\overline{\overline{\varepsilon}}_{eff}$ [51, 52], where d is the slab thickness, ε_0 the vacuum dielectric permittivity, and $\overline{\overline{\varepsilon}}_{eff}$ the effective permittivity tensor calculated from the effective medium approximation [48–50]. To exclude the impact of intrinsic material loss, we omit the real part of $\overline{\overline{\sigma}}$. IFCs are obtained by solving the complex-valued $k_x = k_x' + ik_x''$ for the given purely real k_y values. The detailed calculation process is provided in Supporting Information. The real and imaginary IFCs for the slanted ribbon arrays at $\omega = 1430\,\mathrm{cm}^{-1}$ are displayed in Figs. 2(a), (b), where wavevectors are normalized to $k_0 = 2\pi/\lambda_0$, with λ_0 being the incident free-space wavelength. The oblique angle (φ) relative to the y direction is set equal to the open angle (θ) of the hyperbolic IFCs to the x direction, following $\varphi = \theta = \arctan\sqrt{-\varepsilon_x^{eff}/\varepsilon_y^{eff}} = 34°$. A region (cyan area) in Figs. 2(a), (b) is identified where both k_x' and k_x'' are nonzero, which is caused solely by geometric symmetry breaking, as intrinsic material loss is neglected. Polaritons under this condition exhibit properties of ghost waves, combining characteristics of both propagating and evanescent waves [53–56]. Unlike previous ghost polaritons that propagate and decay within bulk crystals, the polaritons in our configuration are confined along the quasi-one-dimensional interface, which should be referred to as 1DGPs, a polariton realization of ghost line waves at the interface between planar junctions of metasurfaces [57, 58].

However, the presence of 1DGPs alone does not fully satisfy the interfacial matching condition, as there exists a scenario in which the boundary of the 1DGP region remains parallel to the interface normal. Notably, in deriving the IFCs in Fig. 2(a), we neglected the intrinsic material losses. When the real part of $\overline{\overline{\sigma}}$ is included, as is necessary for realistic polaritonic materials, k_x'' increases substantially near the 1DGP region boundary, as shown in Fig. 2(b). This increase in k_x'' reduces k_x', bending the IFCs towards the center. A subregion enclosed by two IFC branches emerges, highlighted by the red region in Fig. 2(c), which we designate as the HL-1DGP region.

For comparison, the real IFCs derived from the well-established waveguide-like dispersion relation of polaritons (Supporting Information) are shown as pink dashed curves in Figs. 2(c), (d). When the transverse axis of the hyperbolic IFC aligns with the y axis (Fig. 2(d), $\varphi = 90°$), the calculated IFC from this method aligns well with the 2D approximation. In contrast, a marked deviation is observed under symmetry breaking, as seen in Fig. 2(c), underscoring the critical role

of HL-1DGPs in understanding the interfacial behavior of hyperbolic polaritons with slanted optical axes.

Utilizing HL-1DGPs allows us to resolve the above paradox in Figs. 1(c), (d). We propose a planar junction of metasurfaces (insets of Figs. 2(c), (d) and investigate the electric field distribution across the planar junction. To reproduce the refraction process, we position a z-polarized dipole on the left side of the interface at 1.5 μm. The real part of the electric field in the z direction, $\mathrm{Re}(E_z)$, is shown in Fig. 2(e), and its Fourier transform (FT) is consistent with the IFCs presented in Figs. 2(c), (d). The directions of the incident ($\mathbf{S_{1h}}$) and refracted Poynting vectors ($\mathbf{S_{2h}}$), extracted from the magnitude of the electric field in Fig. 2(f), agree with the IFC analysis based on high-k modes outside the 1DGP region (black dotted line). Additionally, using IFC analysis within the HL-1DGP region (black dashed line), we identify the energy flows of 1DGPs in Fig. 2(f), denoted by $\mathbf{S_{1g}}$, $\mathbf{S_{2g}}$, and $\mathbf{S_{3g}}$ for the incident, refracted, and reflected waves, respectively. However, these signals are weak and barely observable due to stronger high-k signals.

To more effectively excite 1DGPs, we place the dipole directly at the interface. As expected, polariton modes confined near the interface are observed from the simulation results in Figs. 2(g), (h). Another key observation is the asymmetry in field intensity over the slanted metasurfaces, reflected in an asymmetric FT signal: the field is stronger on one side of the slanted hyperbola, in agreement with the calculated IFCs in Fig. 2(c) but contrasting with the symmetric FT signal in Fig. 2(e). This mirror symmetry breaking is akin to the phenomenon in shear hyperbolic polaritons supported by monoclinic crystals, such as β-Ga_2O_3 [59] and $CdWO_4$ [60], which result from non-orthogonal phonon modes and asymmetric losses in low-symmetry crystals. Consequently, we can conclude that in the case of Fig. 1(c) the reflected polaritons are not forbidden; instead, they transform into HL-1DGPs with their energy dissipating near the interface (y axis). This effect becomes pronounced when the dipole is close to the interface, accompanied by asymmetric field distributions.

We next consider the case in Fig. 1(d). To do so, the hBN ribbon arrays on the right side of the interface are mirrored configurations of those on the left. The corresponding mirrored IFCs are displayed in Figs. 3(a), (b), where the interface normal intersects both the incident and outgoing IFCs within the HL-1DGP subregions. Under these conditions, both reflected and refracted waves convert into HL-1DGPs that decay near the interface. The simulation results in Figs. 3(c), (d) indicate that the transmitted signal is almost undetectable, both in the field distributions and in the FT spectrum (inset). When the point dipole is positioned at the interface, HL-1DGPs appear on both sides, with an asymmetric field intensity within the slanted hyperbola in Figs. 3(e), (f). Such mirror symmetry breaking is similar to that observed in Fig. 2(g), supporting our previous IFC analysis. Although the electric field of HL-1DGPs remains tightly bound to the interface, the canalization effect seen in Figs. 3(e), (f) cannot be attributed solely to HL-1DGPs, as the field intensity here is significantly stronger than in Figs. 2(g), (h). In fact, this strongly canalized field near the interface arises from a combination of HL-1DGPs and canalized polariton modes induced

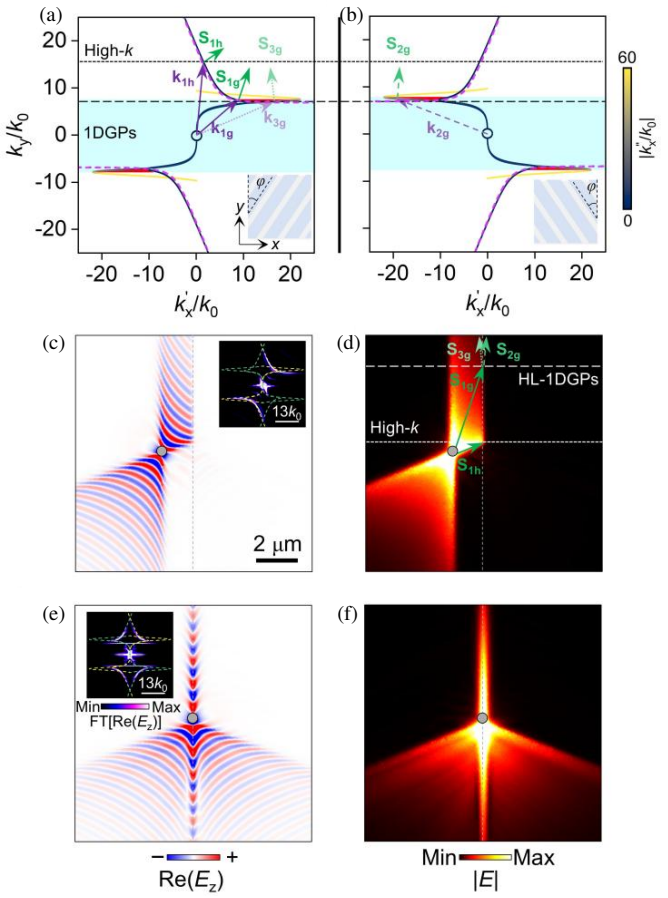

FIGURE 3. Channeling polaritons along the interface using HL-1DGPs. (a), (b) Mirrored IFCs for the incident (a) and outgoing (b) metasurfaces. Inset depicts schematics of the metasurfaces with mirrored configurations relative to the interface (y axis). (c), (d) Simulated field distributions excited by a dipole (gray dot) positioned 1.5 μm to the left of the interface. Inset shows the Fourier transform (FT) signal, which aligns with the calculated incident (yellow) and outgoing (green) IFCs. (e), (f) Same as (c), (d), but with the point dipole placed at the interface.

by the nearly flat IFCs in slanted metasurfaces [50, 61, 62]. The asymmetric field intensity within the two hyperbolic sectors, however, serves as a distinct signature for identifying the formation of HL-1DGPs on both sides in this configuration.

Since polaritons allow energy transport in subwavelength scales, their super-focusing capability is of great interest. Negative refraction of polaritons has been employed to construct planar lenses capable of focusing polaritons with resolutions far beyond the diffraction limit [27, 29, 36]. Building on this mechanism, we design a planar lens composed of two laterally arranged hBN metasurfaces with orthogonal patterns, which is sketched in Fig. 4(a). As expected, the simulated electric field in Fig. 4(b) reveals a focal spot with a linewidth of 0.48 μm $\approx \lambda_0/14.6$. However, this configuration results in significant backscattering, a phenomenon also observed in previous polaritonic lenses based on negative refraction with similar configurations [28]. To mitigate backscattering, we reconstruct the incident part of the structure using two mirrored metasurfaces with $\varphi = \theta$ (Fig. 4(c)). This setup converts reflected waves into HL-1DGPs that dissipate along a direction near the

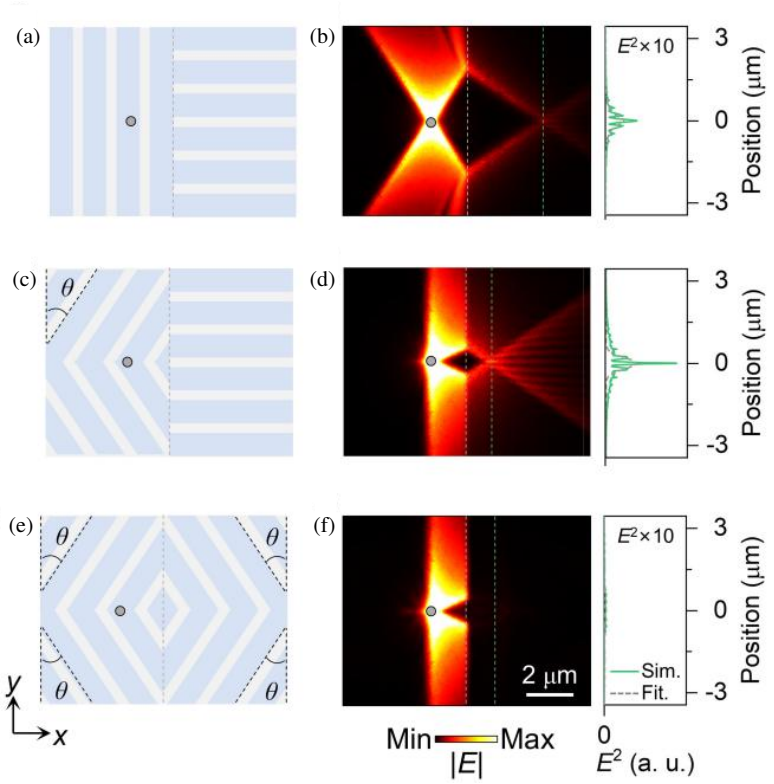

FIGURE 4. Planar polaritonic elements with suppressed backscattering. (a) Schematic of a polaritonic lens based on reflection-accompanied negative refraction, consisting of laterally arranged metasurfaces with orthogonal optical axes. (b) Simulated field distribution (left) and line scan signal (right) along the green dashed line, with the latter fitted using a Lorentzian equation (gray curve). (c), (d) Schematic (c) and field distribution (d) of a reflection-resistant polaritonic lens. (e), (f) Same as (c), (d) but for a reflection-resistant polaritonic absorber, where the transmitted signal is nearly undetectable.

interface, while the negatively refracted polaritons remain unaffected, producing a reflection-resistant polaritonic lens with a linewidth of 0.42 μm $\approx \lambda_0/16.7$ (Fig. 4(d)). This performance is comparable to the lens with reflection in Fig. 4(b). The significantly enhanced field intensity at the focal spot in Fig. 4(d) is primarily caused by the shorter focal length (1 μm) rather than the increased transmission [22], as verified by the simulation results on another reflection-resistant polaritonic lens with a similar focal length (3.35 μm) to that of the lens in Fig. 4(a) (Supporting Information). Although transmission does not appear improved, backscattering is indeed mitigated in this configuration.

In addition to focusing polaritons, we further redirect the refracted polariton flux along the interface by rotating the outgoing metasurfaces clockwise by θ, as shown in Fig. 4(e), where the left and right metasurfaces are symmetric with respect to the interface. In this configuration, both reflected and refracted signals are almost invisible (Fig. 4(f)). The field intensity in Fig. 4(f) is approximately 0.004 times that of the lens in Fig. 4(d) at the same position (focal spot), suggesting that this setup has the potential to function as a quasi-1D absorber for hyperbolic polaritons. Using the same configuration, the polariton canalization can be achieved if the dipole source is placed at the center of the interface, as verified in simulation results in Supporting Information.

Notably, although HL-1DGPs have been employed to solve the paradox in Figs. 1(c), (d), they are not restricted to the specific situation where the asymptotes of the hyperbolic IFCs are critically parallel to the interface normal, i.e., $\varphi = \theta$. Specifically, at $\omega = 1430\,\mathrm{cm}^{-1}$, 1DGPs and HL-1DGPs exist over a broad range of $0° \leq \varphi \leq 44°$, where the existence of 1DGPs is denoted by the finite values of $|k_x'/k_x''|$ (Supporting Information) [58]. When $\varphi > 44°$, 1DGPs vanish and transition into evanescent modes as k' approaches zero. In this case, reflection is physically possible but hardly observable in our simulations. This phenomenon arises from their large wavevectors and narrow coverage [31], following a mechanism fundamentally different from the exotic interfacial behavior based on HL-1DGPs. Comprehensive IFC analyses and simulation results for $0° \leq \varphi \leq 90°$ are provided in Supporting Information.

3. CONCLUSION

In summary, motivated by the phenomenon of negative refraction in hyperbolic polaritons, we identify a specific condition under which one of the asymptotes of hyperbolic IFCs aligns parallel to the interface normal. Our rigorous analysis reveals that HL-1DGPs emerge at interfaces between hyperbolic polaritons with slanted optical axes. Rather than disappearing, the reflected and refracted polariton flows are channeled along the interface. Leveraging this mechanism, we propose the de-

sign of polaritonic lenses and absorbers with reduced reflection. This strategy is also applicable to other artificial or natural hyperbolic polariton systems, such as graphene metasurfaces [48, 63], α-MoO_3 van der Waals layers [51, 64], and β-Ga_2O_3 bulk crystals [59], to name a few. Our findings offer new insights into the interfacial behavior of hyperbolic polaritons under symmetry breaking and hold promise for the design of planar polaritonic elements for subwavelength light control. The configurations proposed here are instructive for the development of polaritonic prisms, lenses, splitters, filters, absorbers, and other refractive elements in polaritonic circuits [65].

ACKNOWLEDGEMENT

The authors acknowledge the support from the National Natural Science Foundation of China (62475228, 62305288 and 62275231), the Key Research and Development Program of the Ministry of Science and Technology (2022YFA1404704, 2022YFA1405200, and 2022YFA1404902), the National Natural Science Foundation of China (62305288), the Key Research and Development Program of Zhejiang Province (2022C01036), and the Fundamental Research Funds for the Central Universities.

REFERENCES

[1] Basov, D. N., M. M. Fogler, and F. J. G. de Abajo, "Polaritons in van der Waals materials," *Science*, Vol. 354, No. 6309, aaag1992, 2016.

[2] Low, T., A. Chaves, J. D. Caldwell, A. Kumar, N. X. Fang, P. Avouris, T. F. Heinz, F. Guinea, L. Martin-Moreno, and F. Koppens, "Polaritons in layered two-dimensional materials," *Nature Materials*, Vol. 16, No. 2, 182–194, 2017.

[3] Zhang, Q., G. Hu, W. Ma, P. Li, A. Krasnok, R. Hillenbrand, A. Alù, and C.-W. Qiu, "Interface nano-optics with van der Waals polaritons," *Nature*, Vol. 597, No. 7875, 187–195, 2021.

[4] Wang, H., A. Kumar, S. Dai, X. Lin, Z. Jacob, S.-H. Oh, V. Menon, E. Narimanov, Y. D. Kim, J.-P. Wang, P. Avouris, L. M. Moreno, J. Caldwell, and T. Low, "Planar hyperbolic polaritons in 2D van der Waals materials," *Nature Communications*, Vol. 15, No. 1, 69, 2024.

[5] Wu, Y., J. Duan, W. Ma, Q. Ou, P. Li, P. Alonso-González, J. D. Caldwell, and Q. Bao, "Manipulating polaritons at the extreme scale in van der Waals materials," *Nature Reviews Physics*, Vol. 4, No. 9, 578–594, 2022.

[6] Galiffi, E., G. Carini, X. Ni, G. Álvarez Pérez, S. Yves, E. M. Renzi, R. Nolen, S. Wasserroth, M. Wolf, P. Alonso-Gonzalez, A. Paarmann, and A. Alù, "Extreme light confinement and control in low-symmetry phonon-polaritonic crystals," *Nature Reviews Materials*, Vol. 9, No. 1, 9–28, 2024.

[7] Ono, M., M. Hata, M. Tsunekawa, K. Nozaki, H. Sumikura, H. Chiba, and M. Notomi, "Ultrafast and energy-efficient all-optical switching with graphene-loaded deep-subwavelength plasmonic waveguides," *Nature Photonics*, Vol. 14, No. 1, 37–43, 2020.

[8] Dolado, I., F. J. Alfaro-Mozaz, P. Li, E. Nikulina, A. Bylinkin, S. Liu, J. H. Edgar, F. Casanova, L. E. Hueso, P. Alonso-González, S. Velez, A. Y. Nikitin, and R. Hillenbrand, "Nanoscale guiding of infrared light with hyperbolic volume and surface polaritons in van der Waals material ribbons," *Advanced Materials*, Vol. 32, No. 9, e1906530, 2020.

[9] He, M., S. I. Halimi, T. G. Folland, S. S. Sunku, S. Liu, J. H. Edgar, D. N. Basov, S. M. Weiss, and J. D. Caldwell, "Guided mid-IR and near-IR light within a hybrid hyperbolic-material/silicon waveguide heterostructure," *Advanced Materials*, Vol. 33, No. 11, e2004305, 2021.

[10] He, M., L. Hoogendoorn, S. Dixit, Z. Pan, G. Lu, K. Diaz-Granados, D. Li, and J. D. Caldwell, "Guided polaritons along the forbidden direction in MoO_3 with geometrical confinement," *Nano Letters*, Vol. 23, No. 11, 5035–5041, 2023.

[11] Yu, S.-J., H. Yao, G. Hu, Y. Jiang, X. Zheng, S. Fan, T. F. Heinz, and J. A. Fan, "Hyperbolic polaritonic rulers based on van der Waals α-MoO_3 waveguides and resonators," *ACS Nano*, Vol. 17, No. 22, 23 057–23 064, 2023.

[12] Alonso-Gonzalez, P., A. Y. Nikitin, F. Golmar, *et al.*, "Controlling graphene plasmons with resonant metal antennas and spatial conductivity patterns," *Science*, Vol. 344, No. 6190, 1369–1373, 2014.

[13] Chaudhary, K., M. Tamagnone, X. Yin, C. M. Spägele, S. L. Oscurato, J. Li, C. Persch, R. Li, N. A. Rubin, L. A. Jauregui, *et al.*, "Polariton nanophotonics using phase-change materials," *Nature Communications*, Vol. 10, No. 1, 4487, 2019.

[14] Zhao, Y., G. Li, Y. Yao, J. Chen, M. Xue, L. Bao, K. Jin, C. Ge, and J. Chen, "Tunable heterostructural prism for planar polaritonic switch," *Science Bulletin*, Vol. 68, No. 16, 1757–1763, 2023.

[15] Folland, T. G., A. Fali, S. T. White, J. R. Matson, S. Liu, N. A. Aghamiri, J. H. Edgar, R. F. H. Jr., Y. Abate, and J. D. Caldwell, "Reconfigurable infrared hyperbolic metasurfaces using phase change materials," *Nature Communications*, Vol. 9, No. 1, 4371, 2018.

[16] Duan, J., G. Álvarez Pérez, A. I. F. Tresguerres-Mata, J. Taboada-Gutiérrez, K. V. Voronin, A. Bylinkin, B. Chang, S. Xiao, S. Liu, J. H. Edgar, J. I. Martín, V. S. Volkov, R. Hillenbrand, J. Martín-Sánchez, A. Y. Nikitin, and P. Alonso-González, "Planar refraction and lensing of highly confined polaritons in anisotropic media," *Nature Communications*, Vol. 12, No. 1, 4325, 2021.

[17] Martín-Sánchez, J., J. Duan, J. Taboada-Gutiérrez, *et al.*, "Focusing of in-plane hyperbolic polaritons in van der Waals crystals with tailored infrared nanoantennas," *Science Advances*, Vol. 7, No. 41, eabj0127, 2021.

[18] Zheng, Z., J. Jiang, N. Xu, X. Wang, W. Huang, Y. Ke, S. Zhang, H. Chen, and S. Deng, "Controlling and focusing in-plane hyperbolic phonon polaritons in α-MoO_3 with a curved plasmonic antenna," *Advanced Materials*, Vol. 34, No. 6, e2104164, 2022.

[19] Qu, Y., N. Chen, H. Teng, H. Hu, J. Sun, R. Yu, D. Hu, M. Xue, C. Li, B. Wu, *et al.*, "Tunable planar focusing based on hyperbolic phonon polaritons in α-MoO_3," *Advanced Materials*, Vol. 34, No. 23, e2105590, 2022.

[20] Ma, L., A. Ge, L. Sun, F. Liu, and W. Lu, "Focusing of hyperbolic phonon polaritons by bent metal nanowires and their polarization dependence," *ACS Photonics*, Vol. 10, No. 6, 1841–1849, 2023.

[21] Cui, Z., S. Xia, L. Shen, B. Zheng, H. Chen, and Y. Wu, "Polariton microfluidics for nonreciprocal dragging and reconfigurable shaping of polaritons," *Nano Letters*, Vol. 24, No. 4, 1360–1366, 2024.

[22] Wu, Y., J. Liu, W. Yu, T. Zhang, H. Mu, G. Si, Z. Cui, S. Lin, B. Zheng, C.-W. Qiu, H. Chen, and Q. Ou, "Monolithically structured van der Waals materials for volume-polariton refraction and focusing," *ACS Nano*, Vol. 18, No. 26, 17 065–17 074, 2024.

[23] Ding, F., "A review of multifunctional optical gap-surface plasmon metasurfaces," *Progress In Electromagnetics Research*,

Vol. 174, 55–73, 2022.

[24] Pendry, J. B., "Negative refraction makes a perfect lens," *Physical Review Letters*, Vol. 85, No. 18, 3966, 2000.

[25] Shin, H. and S. Fan, "All-angle negative refraction for surface plasmon waves using a metal-dielectric-metal structure," *Physical Review Letters*, Vol. 96, No. 7, 073907, 2006.

[26] Liu, Y., G. Bartal, and X. Zhang, "All-angle negative refraction and imaging in a bulk medium made of metallic nanowires in the visible region," *Optics Express*, Vol. 16, No. 20, 15 439–15 448, 2008.

[27] Lin, X., Y. Yang, N. Rivera, J. J. López, Y. Shen, I. Kaminer, H. Chen, B. Zhang, J. D. Joannopoulos, and M. Soljačić, "All-angle negative refraction of highly squeezed plasmon and phonon polaritons in graphene-boron nitride heterostructures," *Proceedings of the National Academy of Sciences*, Vol. 114, No. 26, 6717–6721, 2017.

[28] Jiang, J., X. Lin, and B. Zhang, "Broadband negative refraction of highly squeezed hyperbolic polaritons in 2D materials," *Research*, Vol. 2018, 2532819, 2018.

[29] Zhang, Q., Z. Zhen, C. Liu, D. Jariwala, and X. Cui, "Gate-tunable polariton superlens in 2D/3D heterostructures," *Optics Express*, Vol. 27, No. 13, 18 628–18 641, 2019.

[30] Zhang, Q., Z. Zhen, Y. Yang, G. Gan, D. Jariwala, and X. Cui, "Negative refraction inspired polariton lens in van der Waals lateral heterojunctions," *Applied Physics Letters*, Vol. 114, No. 22, 221101, 2019.

[31] Zhang, T., C. Zheng, Z. N. Chen, and C.-W. Qiu, "Negative reflection and negative refraction in biaxial van der Waals materials," *Nano Letters*, Vol. 22, No. 13, 5607–5614, 2022.

[32] Liu, R.-T. and C.-C. Huang, "Interfacing differently oriented biaxial van der Waals crystals for negative refraction," *Nanophotonics*, Vol. 12, No. 21, 4063–4072, 2023.

[33] Liu, R.-T., Y.-Z. Wu, and C.-C. Huang, "Focusing of mid-infrared polaritons through patterned graphene on van der Waals crystals," *Nanophotonics*, Vol. 13, No. 15, 2753–2763, 2024.

[34] Chen, Q., Y. Yang, L. Zhang, J. Chen, M. Li, X. Lin, R. Li, Z. Wang, B. Zhang, and H. Chen, "Negative refraction of ultra-squeezed in-plane hyperbolic designer polaritons," *Photonics Research*, Vol. 9, No. 8, 1540–1549, 2021.

[35] Hu, H., N. Chen, H. Teng, R. Yu, Y. Qu, J. Sun, M. Xue, D. Hu, B. Wu, C. Li, *et al.*, "Doping-driven topological polaritons in graphene/α-MoO_3 heterostructures," *Nature Nanotechnology*, Vol. 17, No. 9, 940–946, 2022.

[36] Hu, H., N. Chen, H. Teng, R. Yu, M. Xue, K. Chen, Y. Xiao, Y. Qu, D. Hu, J. Chen, *et al.*, "Gate-tunable negative refraction of mid-infrared polaritons," *Science*, Vol. 379, No. 6632, 558–561, 2023.

[37] Sternbach, A. J., S. L. Moore, A. Rikhter, S. Zhang, R. Jing, Y. Shao, B. S. Y. Kim, S. Xu, S. Liu, J. H. Edgar, *et al.*, "Negative refraction in hyperbolic hetero-bicrystals," *Science*, Vol. 379, No. 6632, 555–557, 2023.

[38] He, H., C. Qiu, L. Ye, X. Cai, X. Fan, M. Ke, F. Zhang, and Z. Liu, "Topological negative refraction of surface acoustic waves in a Weyl phononic crystal," *Nature*, Vol. 560, No. 7716, 61–64, 2018.

[39] Liu, Y., G. P. Wang, J. B. Pendry, and S. Zhang, "All-angle reflectionless negative refraction with ideal photonic Weyl metamaterials," *Light: Science & Applications*, Vol. 11, No. 1, 276, 2022.

[40] Yu, Z., S. Lin-Fang, R. Li-Xin, C. Xu-Dong, L. Jylhä, T. M. Grzegorczyk, and J. A. Kong, "Reflection and refraction on the boundary of a left-handed material with a hyperbolic dispersion relation," *Chinese Physics Letters*, Vol. 23, No. 5, 1296–1298, 2006.

[41] Guo, Z., H. Jiang, and H. Chen, "Abnormal wave propagation in tilted linear-crossing metamaterials," *Advanced Photonics Research*, Vol. 2, No. 1, 2000071, 2021.

[42] Deriy, I., K. Lezhennikova, S. Glybovsky, I. Iorsh, O. Yermakov, M. Song, R. Abdeddaim, S. Enoch, P. Belov, and A. Bogdanov, "Anomalous reflection from hyperbolic media," *ArXiv Preprint ArXiv:2308.10495*, 2023.

[43] Voronin, K. V., G. Álvarez Pérez, C. Lanza, P. Alonso-González, and A. Y. Nikitin, "Fundamentals of polaritons in strongly anisotropic thin crystal layers," *ACS Photonics*, Vol. 11, No. 2, 550–560, 2024.

[44] Fang, A., T. Koschny, and C. M. Soukoulis, "Optical anisotropic metamaterials: Negative refraction and focusing," *Physical Review B*, Vol. 79, No. 24, 245127, 2009.

[45] Lezec, H. J., J. A. Dionne, and H. A. Atwater, "Negative refraction at visible frequencies," *Science*, Vol. 316, No. 5823, 430–432, 2007.

[46] Valentine, J., S. Zhang, T. Zentgraf, E. Ulin-Avila, D. A. Genov, G. Bartal, and X. Zhang, "Three-dimensional optical metamaterial with a negative refractive index," *Nature*, Vol. 455, No. 7211, 376–379, 2008.

[47] Shah, S., Y. Jiang, L. Song, H. Wang, and L. Shen, "Optical axis-driven field discontinuity in a hyperbolic medium," *Optics Letters*, Vol. 45, No. 11, 3067–3070, 2020.

[48] Gomez-Diaz, J. S., M. Tymchenko, and A. Alù, "Hyperbolic plasmons and topological transitions over uniaxial metasurfaces," *Physical Review Letters*, Vol. 114, No. 23, 233901, 2015.

[49] Li, P., I. Dolado, F. J. Alfaro-Mozaz, *et al.*, "Infrared hyperbolic metasurface based on nanostructured van der Waals materials," *Science*, Vol. 359, No. 6378, 892–896, 2018.

[50] Li, P., G. Hu, I. Dolado, M. Tymchenko, C.-W. Qiu, F. J. Alfaro-Mozaz, F. Casanova, L. E. Hueso, S. Liu, J. H. Edgar, *et al.*, "Collective near-field coupling and nonlocal phenomena in infrared-phononic metasurfaces for nano-light canalization," *Nature Communications*, Vol. 11, No. 1, 3663, 2020.

[51] Ma, W., P. Alonso-González, S. Li, A. Y. Nikitin, J. Yuan, J. Martín-Sánchez, J. Taboada-Gutiérrez, I. Amenabar, P. Li, S. Vélez, *et al.*, "In-plane anisotropic and ultra-low-loss polaritons in a natural van der Waals crystal," *Nature*, Vol. 562, No. 7728, 557–562, 2018.

[52] Hu, G., Q. Ou, G. Si, Y. Wu, J. Wu, Z. Dai, A. Krasnok, Y. Mazor, Q. Zhang, Q. Bao, C.-W. Qiu, and A. Alù, "Topological polaritons and photonic magic angles in twisted α-MoO_3 bilayers," *Nature*, Vol. 582, No. 7811, 209–213, 2020.

[53] Narimanov, E., "Ghost resonance in anisotropic materials: Negative refractive index and evanescent field enhancement in lossless media," *Advanced Photonics*, Vol. 1, No. 4, 046003, 2019.

[54] Ma, W., G. Hu, D. Hu, R. Chen, T. Sun, X. Zhang, Q. Dai, Y. Zeng, A. Alù, C.-W. Qiu, and P. Li, "Ghost hyperbolic surface polaritons in bulk anisotropic crystals," *Nature*, Vol. 596, No. 7872, 362–366, 2021.

[55] Zhang, Q., S.-P. Hao, H.-Y. Song, H.-Y. Peng, S.-F. Fu, and X.-Z. Wang, "Unique ghost surface phonon polaritons in biaxially hyperbolic materials," *Optics Express*, Vol. 31, No. 26, 43 821–43 837, 2023.

[56] Yan, Q., D. Lu, Q. Chen, X. Luo, M. Xu, Z. Zhang, X. Yang, X. Zhang, and P. Li, "Hybrid ghost phonon polaritons in thin-film heterostructure," *Nano Letters*, Vol. 24, No. 15, 4346–4353, 2024.

[57] Moccia, M., G. Castaldi, A. Alù, and V. Galdi, "Line waves in non-Hermitian metasurfaces," *ACS Photonics*, Vol. 7, No. 8, 2064–2072, 2020.

[58] Moccia, M., G. Castaldi, A. Alù, and V. Galdi, "Ghost line waves," *ACS Photonics*, Vol. 10, No. 6, 1866–1872, 2023.

[59] Passler, N. C., X. Ni, G. Hu, J. R. Matson, G. Carini, M. Wolf, M. Schubert, A. Alù, J. D. Caldwell, T. G. Folland, and A. Paarmann, "Hyperbolic shear polaritons in low-symmetry crystals," *Nature*, Vol. 602, No. 7898, 595–600, 2022.

[60] Hu, G., W. Ma, D. Hu, J. Wu, C. Zheng, K. Liu, X. Zhang, X. Ni, J. Chen, X. Zhang, *et al.*, "Real-space nanoimaging of hyperbolic shear polaritons in a monoclinic crystal," *Nature Nanotechnology*, Vol. 18, No. 1, 64–70, 2023.

[61] Correas-Serrano, D., A. Alù, and J. S. Gomez-Diaz, "Plasmon canalization and tunneling over anisotropic metasurfaces," *Physical Review B*, Vol. 96, No. 7, 075436, 2017.

[62] Xing, Q., J. Zhang, Y. Fang, C. Song, T. Zhao, Y. Mou, C. Wang, J. Ma, Y. Xie, S. Huang, *et al.*, "Tunable anisotropic van der Waals films of 2M-WS_2 for plasmon canalization," *Nature Communications*, Vol. 15, No. 1, 2623, 2024.

[63] Hu, G., A. Krasnok, Y. Mazor, C.-W. Qiu, and A. Alu, "Moiré hyperbolic metasurfaces," *Nano Letters*, Vol. 20, No. 5, 3217–3224, 2020.

[64] Zheng, Z., N. Xu, S. L. Oscurato, M. Tamagnone, F. Sun, Y. Jiang, Y. Ke, J. Chen, W. Huang, W. L. Wilson, *et al.*, "A mid-infrared biaxial hyperbolic van der Waals crystal," *Science Advances*, Vol. 5, No. 5, eaav8690, 2019.

[65] Yao, D., P. H. He, H. Zhang, J. Zhu, M. Hu, and T.-J. Cui, "Miniaturized photonic and microwave integrated circuits based on surface plasmon polaritons," *Progress In Electromagnetics Research*, Vol. 175, 105–125, 2022.